ANALYTICAL MODELING OF HELIUM TURBOMACHINERY USING FORTRAN 77

by

PURUSHOTHAM BALAJI

Presented to the Faculty of the Graduate School of

The University of Texas at Arlington in Partial Fulfillment

of the Requirements

for the Degree of

MASTER OF SCIENCE IN AEROSPACE ENGINEERING

THE UNIVERSITY OF TEXAS AT ARLINGTON

DECEMBER 2015

Acknowledgements

I wish to express my sincere appreciation to my supervising professor, Dr. Donald R Wilson, for his guidance, support and recommendations throughout the course of this research work. I also wish to thank Dr. Brian Dennis and Dr. Abdolhossein Haji-Sheikh for serving as members of my committee.

I would like to thank my fellow-workers Hatim Rangwala, Freitas and Gopal at the Aerodynamics Research Center for their support, cooperation and friendship. Special thanks to my parents for their care and support.

December 7, 2015

Abstract

ANALYTICAL MODELING OF HELIUM TURBOMACHINERY USING FORTRAN77

Purushotham Balaji, MS

The University of Texas at Arlington, 2015

Supervising Professor: Donald R. Wilson

Advanced Generation IV modular reactors, including Very High Temperature Reactors (VHTRs), utilize helium as the working fluid, with a potential for high efficiency power production utilizing helium turbomachinery. Helium is chemically inert and nonradioactive which makes the gas ideal for a nuclear power-plant environment where radioactive leaks are a high concern. These properties of helium gas helps to increase the safety features as well as to decrease the aging process of plant components.

The lack of sufficient helium turbomachinery data has made it difficult to study the vital role played by the gas turbine components of these VHTR powered cycles. Therefore, this research work focuses on predicting the performance of helium compressors. A FORTRAN77 program is developed to simulate helium compressor operation, including surge line prediction.

The resulting design point and off design performance data can be used to develop compressor map files readable by Numerical Propulsion Simulation Software (NPSS). This multi-physics simulation software that was developed for propulsion system analysis has found applications in simulating power-plant cycles.

Table of Contents

List of Illustrations

List of Tables

List of Symbols

a	maximum blade camber
A	cross sectional flow area (m^2)
C	Blade chord
C_p	specific heat at constant pressure
C_V	Specific heat at constant volume
D	diameter
	diffusion ratio
ΔP_{loss}	total pressure losses
g	acceleration of gravity
H	blade height
h	enthalpy
i	blade incidence angle (degrees)
$\dot{m}$	mass flow rate
M	Mach number
n	iteration number
P	gas pressure
r	radius
R	rotor
Re	Reynold's number
R_n	degree of reaction

s	blade spacing
S	stator
t_{max}	maximum blade thickness
T	temperature
U	blade Speed
V	absolute gas velocity
W	relative gas velocity
$\dot{W}$	power [required/delivered] in Watts
Y	pressure loss coefficient
Z	compressibility factor

Greek

α	absolute gas flow angle (degrees)
β	blade angle (degrees)
μ	dynamic viscosity
Φ_f	flow coefficient
ψ	loading coefficient
φ	relative gas flow angle (degrees)
λ	blade setting angle or stagger angle (degrees)
θ	blade camber angle (degrees)

σ	blade solidity
δ	flow deviation angle (degrees)
ρ	gas density
Γ	circulation parameter

Subscripts

0	stagnation condition
	station 0 of blade passage contraction zone
	0 camber angle blade profile
1	leading edge station number
2	trailing edge station number
in	compressor inlet
ex	compressor exit
x	axial component
θ	polar component
AOA	angle of attack
s	stator
	positive stall
c	negative stall
C	compressor
eq	equivalent

max	maximum possible value
m	mean
min	minimum possible value

Superscripts

*	design point condition
	optimum condition
disk	rotating component
n	iteration number

Chapter 1

Introduction

Industrial gas turbines have been used for many years to generate power and other important industrial applications. They consist of an air compressor driven by a turbine which produces power. The succesful operation at high efficiency is the result of complex interactions between the compressor and turbine, their respective sub-components and combustion systems. In nuclear power-plants the combustion system (or) the heating unit is a controlled nuclear fission reaction enclosed by a sheild meeting environmental safety standards. A schematic for a natural gas-fired power-plant operating in a combined cycle mode is shown below,

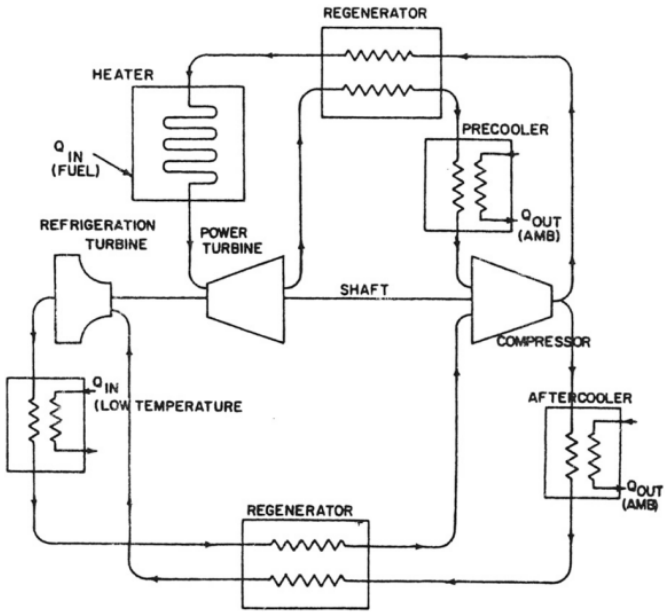

Figure 1-1: Cycle Diagram of La Fleur Helium Gas Turbine Plant [16]

Proper application of the compressor includes consideration of the plant elevation, ambient conditions and the power requirements. In this research the compression unit of

the Brayton cycle is modelled using a computer program to study the helium compressor's performance.

1.1 Helium as a Working Fluid

The fossil-fired gas turbines with air as the working fluid delivered favorable performance for a maximum power requirement of 30 MWe [16].The demand for higher efficiencies and power requirements of the closed Brayton cycles increased due to the increased global energy needs. Therefore gases other than air were taken into consideration to inspect the feasibility of high efficiency large power plants.

Professor Ackeret, co-founder of the closed Brayton cycle, was the first one to suggest the coupling of a high temperature gas-cooled nuclear reactor with a closed-cycle gas turbine power conversion system using helium in 1945 [16]. Various studies done in the past 70 decades concluded that helium is the best candidate among other possible candidates such as carbon dioxide, nitrogen and various other gas mixtures [16]. Helium satisfies two of the most important design aspects for a closed cycle nuclear power-plant.

Engineering Aspects [17]:

- The helium as a gas has a higher heat transfer coefficient, so that it is able to absorb heat much more quickly and efficiently as compared to water.
- Helium as an inert gas in a nuclear reaction to help increase safety features as well as to decrease the aging process of the components.
- Having a single phase reactor can have tremendous advantages, as the whole system can be designed with the single phase constraints.

. Environmental Aspects [17]:

- The emissions caused by fossil-fired power-plants are a major concern . In helium cooled reactors there are no carbon dioxide emissions.

- Being non radioactive, the chances of radioactive contamination during operation of the power plant is virtually zero.

Thus the above discussed advantages makes helium the best candidate for a high thermal efficient power production concept satisfying desired safety requirements. Table 1-1 is a summary of the previous helium turbomachines' salient features [16].

However the challenges faced during the aerodynamic design of helium turbomachines needs to be addressed. The Euler turbine equation [18] is given as,

$$T_{0\,\mathrm{ex}} - T_{0\,\mathrm{in}} = \frac{U}{C_p}[V_{2x}tan\alpha_2 - V_{1x}tan\alpha_1]$$

$$C_p = \begin{cases} 5195\,\dfrac{J}{kgK}\ [Helium] \\ 1004\,\dfrac{J}{kgK}\ [Air] \end{cases}$$

This difference in the specific heat values reduces the total temperature rise across a helium compressor stage to one-fifth of the total temperature rise across an air compressor stage for the same geometry and flow turning produced. Therefore the resulting compressor design of a helium compressor includes a large number of stages to achieve the required pressure rise.

1.2 Motivation

This power production concept described in the previous section has the potential for satisfying the large-scale and clean energy production needs. Thus predicting the performance of these plants' components is an important step to be taken before performing actual or experimental tests. High fidelity CFD solvers calibrated with test results [1] were also developed. But employing these models for a first level analysis is quite time consuming and a tedious process. Hence a lower order analytical model would best fit this purpose.

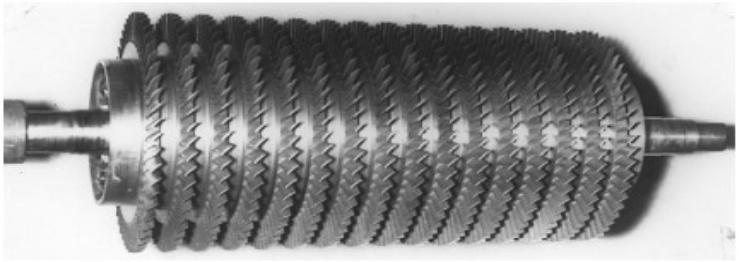

Figure 1-2: 16-Stage Helium Compressor; pressure ratio: 1.5 (La Fleur Corp.) [16]

Table 1-1: Summary of Operated Helium Turbomachinery Facilities [16]

Turbomachine	Helium closed-cycle gas turbines			Test facility	Helium circulator
Facility	La Fleur gas turbine	Escher Wyss gas turbine	Oberhausen 11 power plant	HHV test loop	FSV HTGR
Country	USA	USA	Germany	Germany	USA
Year	1962	1966	1974	1981	1976
Application	Cryogenic	Cryogenic	CHP plant	Development	Nuclear plant
Heat source	NG	NG	Coke oven gas	Electrical	Nuclear
Power, MW	2 equiv.	6 equiv.	50	90	4
Cycle	Recuperated	ICR	ICR	Customized	Steam
Compressor					
Type	Axial	Axial	Axial	Axial	Axial
No. stages	16	10LP,8HP	10LP,15HP	8	1
Inlet press. MPa	1.25	1.22	1.05,2.85	4.5	4.73
Inlet temp. °C	21	22	25	820	394
Pressure ratio	1.5	2.0	2.7l	1.13	1.02
Flow, kg/sec	7.3	11	85	212	110
In vol. flow, m^3/sec	3.5	5.5	50	107	32
Turbine					
Type	Axial	Axial	Axial	Axial	ST
No. stages	4	9	11LP,7HP	2	1
Inlet press. MPa	1.8	2.3	1.65	5.0	–
Inlet temp. °C	650	660	750	850	–
In vol. flow, m^3/sec	3.0	5.7	67	98	–
Out vol. flow, m^3/sec	3.6	8.5	120	104	–
Rotation speed, rpm	19,500	18,000	5500/3000	3000	9550
Shaft type	Single	Single	Twin (geared)	Single	Single
Generator type	None	None	Conventional	Elect. motor	–

Therefore an analytical model “HeComp” was developed using FORTRAN 77 language. This code has an average computation time of 2 seconds and a global convergence criterion of 10E-9. The user has to specify the geometry of the compressor, inlet conditions and blade geometry. If the blade alignment is not known a separate program “BladeDesign” can be used to determine the optimum blade alignment for the given stage performance parameters.

1.3 Code Validation

JAEA's[Japan Atomic Energy Agency] is developing a single shaft helium gas turbine to increase the efficiency of the HTTR reactor. The nuclear helium gas turbine rated at 300 MWe has a 20-stage axial compressor and a 6-stage turbine. To study the aerodynamic design of this compressor, a prototype compressor was built for experimental purposes. This test compressor is a 4-stage axial compressor driven by a 3.65 MW motor [1].

Literature [1] is a presentation of the experimental results reported on the test compressor's performance. These test results were used to calibrate a 3-D viscous CFD model which is a high fidelty tool designed to study the full scale helium compressor. This is the only literature that contains experimental results on helium compressor with advanced aerodynamic design features [1]. The performance prediction by the 3-D CFD simulation for the 20-stage compressor is also presented by Yan et al [1].

Hence the code developed in this research is used to simulate the experimental 4-stage axial compressor performance operation [1] for validation purposes. The analytical model developed by this writer is also compared with the test-calibrated CFD results of both the test compressor and the full compressor.

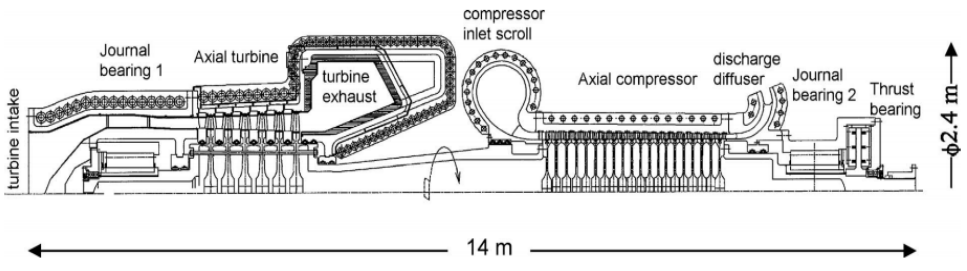

Figure 1-3: 300 MWe Nuclear Helium Gas Turbine by JAEA [1]

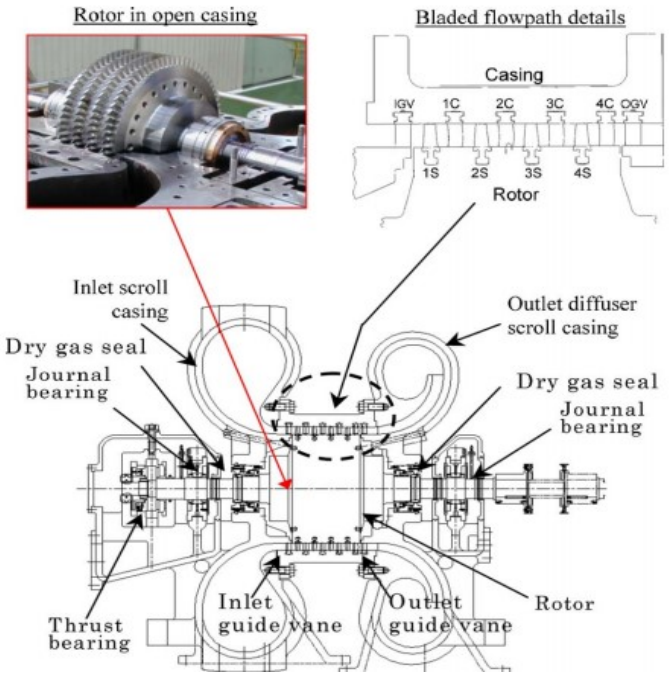

Figure 1-4: 4-Stage Axial Test Compressor [1]

Chapter 2

Blade Design

The following section describes the aerodynamic design procedure required to determine the blade angles corresponding to the design parameters of the GTHTR300 test compressor [1]. The test compressor is 1/3 scale model of the full compressor and it has a rotational speed of 10800 RPM and a mass flow rate of 12.20 kg/s at design point to achieve the full scale compressor's tip speed of 321 m/s at the first rotor stage, refer to Table 2-1 for design requirements.

The low subsonic nature of this compressor allows the use of the NACA 65-series ($t_{max}/C = 0.1$, $a/C = 0.5$) blade profile for which there are numerous 2-dimensional cascade data [7] [2]. The empirical models derived from the experimental data of the same blade profile address the fluid turning and off-design flow fields more accurately.

2.1 Dimensionless Stage Performance Parameters

The flow coefficient Φ_f and loading coefficient ψ are given in Table 2.1. The definition of loading coefficient changes from author to author. In order to be compatible with the stage design model described by Dixon [4], the loading coefficient becomes 0.315(0.63/2) [5]. The degree of reaction is not stated in Table 2.1. Previous CFD simulations showed that a value of 0.8 resulted in comparable results with the experimental results of the helium compressor test facility [8].

2.1.1 Flow Coefficient, Φ_f

The ratio of axial flow velocity to the blade speed is known as the flow coefficient (Φ_f) or the flow capacity of the stage. It is given by the formula,

$$\Phi_f = \frac{V_x}{U} \qquad 2.1$$

2.1.2 Loading Coefficient, ψ

The loading coefficient is the dimensionless work done per stage and is derived from the Euler turbine equation. The work coefficient or loading coefficient is negative for compressors, fans and pumps as work is delivered from other components like turbines for which the loading coefficient is positive.

$$\psi = -\frac{g_c(h_{02} - h_{01})}{U^2} = -\frac{V_{2\theta} - V_{1\theta}}{U} \quad 2.2$$

2.1.3 Degree of Reaction, R_n

The ratio of change in static enthalpy to the change in total or stagnation enthalpy of the gas passing through the rotor is the common definition of stage reaction or degree of reaction, R_n.

$$R_n = \frac{h_2 - h_1}{h_{02} - h_{01}} \quad 2.3$$

It has an important influence on stage efficiency; a reaction of 0.5 minimizes the tendency of the blade boundary layers to separate from the solid surface, thus avoiding large stagnation pressure losses [5]. Stage reaction can also be defined as the change in static pressure to the change in stagnation pressure. Figure 2-1 shows the velocity diagrams corresponding to $R_n < 50\%$ and $R_n > 50\%$ [4]. The present design requirement has a reaction of 0.80. This means that 80 % of static enthalpy rise in a stage is from the rotor blade passage.

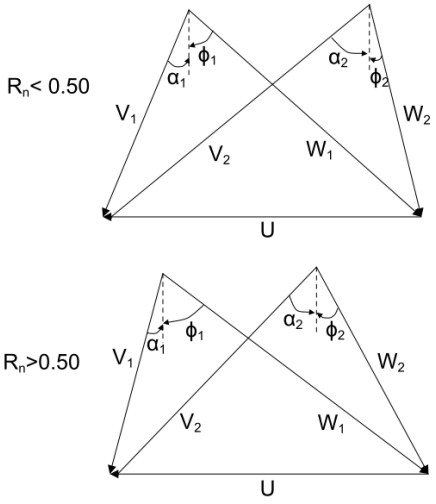

Figure 2-1: Velocity diagrams for different values of stage reaction, R_n

Table 2-1: Design parameters for full and test compressors [1]

	Full compressor	Test compressor
Nominal design conditions		
Inlet pressure (MPa)	3.52	0.883
Inlet temperature (°C)	28.4	30
Pressure ratio, flange to flange	2.0	1.15
Mass flow (kg/s)	442	12.2
Rated speed (rmp)	3,600	10,800
Aerodynamic design pitch line values		
Number of stages	20	4
Tip diameter (first rotor) (m)	1.70	0.57
Hub diameter (first stator) (m)	1.50	0.50
Tip speed (first stage) (m/s)	321	321
Rotar/stator blade count (first stage)	72/94	72/94
Rotar/stator chord (first stage) (mm)	78/60	26/20
Rotar/stator solidity (first stage)	1.19/1.20	1.19/1.20
Rotar/stator aspect ratio (first stage)	1.3/1.7	1.3/1.7
Rotar tip/stator hub clearance	~1% blade span	~1% blade span
Flow coefficient	0.51	0.51
Load coefficient	0.63	0.63
Reaction	High reaction	High reaction

2.2 Velocity Triangles

For a repeating stage design, the velocity triangles can be specified in terms of the dimensionless parameters described above. Using simple trigonometric identities, the relative and absolute gas flow angles can be calculated as follows [4],

$$R_n = \frac{1}{2} + \frac{(tan\Phi_2 - tan\alpha_1)\Phi_f}{2} \quad (2.4)$$

$$\psi = 1 - \Phi_f(tan\alpha_1 + tan\Phi_2) \quad (2.5)$$

$$\phi_f = \frac{1}{tan\alpha_1 + tan\phi_1} = \frac{1}{tan\alpha_2 + tan\phi_2} \quad (2.6)$$

Table 2-2: Rotor relative and absolute flow angles

$R_n = 0.80, \quad \phi_f = 0.51, \quad \psi = 0.315$			
ϕ_1	61.95	α_1	4.76
ϕ_2	51.55	α_2	35.02

Once the flow angles are calculated we can proceed with the blade design procedure explained by Aungier [2]. However, basic geometric parameters like solidity, location of maximum camber and maximum thickness as a percent of chord would be needed to determine the blade design.

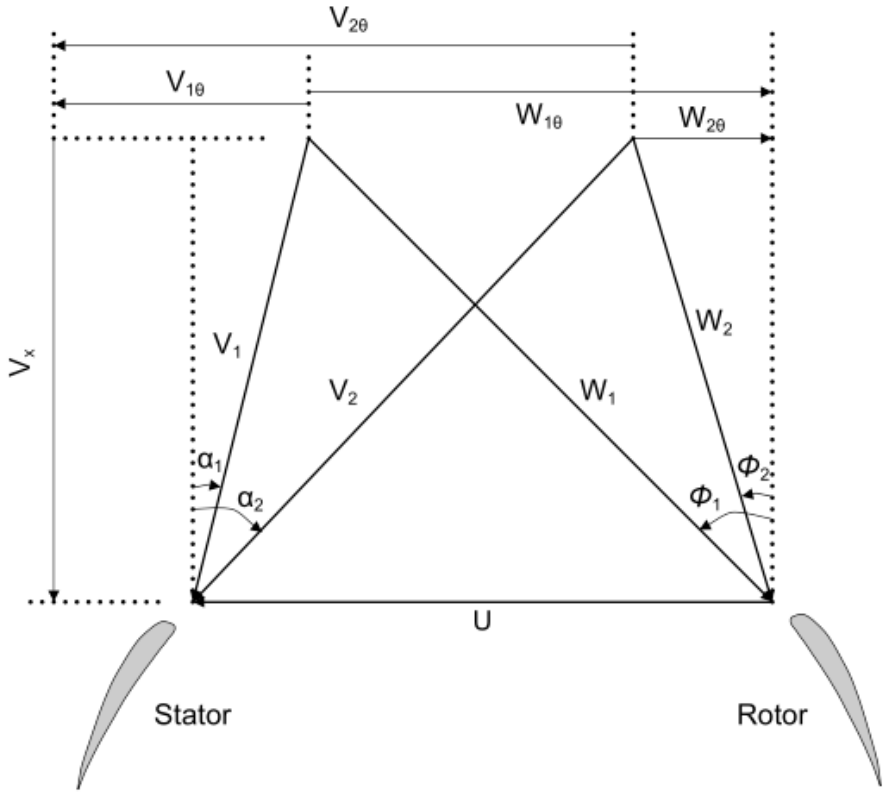

Figure 2-2: Combined velocity triangle

2.3 Blade Angle Solution Technique

The cascade data of the NACA-65 series blades from Herrig [7] was used by Lieblein [3] and Aungier [2] to develop empirical models to calculate the design point/near-optimum angle of attack, incidence angle and the deviation angle in degrees.

2.3.1 Design Angle of Attack, α^*

The angle between the inlet flow angle and stagger angle (λ) is called the angle of attack.

$$\alpha_{AOA} = \phi_1 - \lambda \qquad 2.7$$

The design angle of attack is one which has a smooth blade surface distribution particularly on the suction side. Aungier [2] formulated an empirical model based on the cascade data by Herrig [7].

$$\alpha_{AOA}^{*} = \left[3.6K_{sh}K_{ti} + 0.3532\theta\left(\frac{a}{c}\right)^{0.25}\right]\sigma^{0.65-0.002\theta} \qquad 2.8$$

$$K_{sh} = K_{ti} = 1.0$$

The blade shape parameter (K_{sh}) and the design incidence angle thickness correction factor (K_{ti}) for any blade profiles other than NACA-65 series with a/C = 0.5 and t_{max}/C= 0.1 are defined as follows,

$$K_{sh} = \begin{cases} 1.0 \ (NACA\ profiles) \\ 1.1\ (c4 - series) \\ 0.7\ (double - circular - arc\ profiles) \end{cases}$$

An empirical model for K_{ti} was developed by Lieblein [3] and it's defined by,

$$K_{ti} = 10(\frac{t_{max}}{C})^{q} \qquad 2.9$$

$$q = \frac{0.28}{0.1 + (\frac{t_{max}}{C})^{0.3}}$$

2.3.2 Design Incidence Angle, i^{*}

The angle between the inlet velocity vector and the blade inlet angle is known as the incidence angle, refer to Figure 2-3 for the blade nomenclature.

$$i = \phi_1 - \beta_1 \qquad 2.10$$

A design incidence angle is the incidence angle which corresponds to a minimum loss profile for the cascade operation. Lieblein's correlation [3] is,

$$i^{*} = K_{sh}K_{ti}(i_0^{*})_{10} + n\theta \qquad 2.11$$

Parameter n is the slope factor which can be calculated using the following empirical relation [3] [6],

$$n = 0.025\sigma - 0.06 - \frac{\left(\frac{\phi_1}{90}\right)^{1+1.2\sigma}}{1.5 + 0.43\sigma}$$

The term $(i_0^*)_{10}$ is the design incidence angle for a camber angle(θ) of zero. The subscript 10 corresponds to the values of design incidence angles for 10% maximum-thickness ratio.

$$(i_0^*)_{10} = \frac{\phi_1^{\left(0.914+\frac{\sigma^3}{160}\right)}}{5 + 46\exp(-2.3\sigma)} - 0.1\sigma^3 \exp\left[\frac{\phi_1 - 70}{4}\right]$$

The relation between design incidence angle and the design angle of attack is given by

$$i^* = \alpha^* + \lambda - \beta_1 \qquad 2.12$$

More accurate predictions were reported for the design angle of attack model than the design incidence angle model [2].

2.3.3 Design Deviation Angle, δ^*

Deviation angle δ is the angle between the exit velocity vector and the blade angle at the trailing edge.

$$\delta = \phi_2 - \beta_2 \qquad 2.13$$

Lieblein [3] has formulated an empirical model which defines the design deviation angle as follows

$$\delta^* = K_{sh}K_{t\delta}(\delta_0^*)_{10} + m\theta \qquad 2.14$$

The base zero-camber deviation angle $(\delta_0^*)_{10}$ [3] is defined as [6],

$$(\delta_0^*)_{10} = 0.01\sigma\phi_1 + [0.74\sigma^{1.9} + 3\sigma]\left(\frac{\phi_1}{90}\right)^{1.67+1.09\sigma}$$

The slope parameter m, [2] [6] is expressed as,

$$m = \frac{0.17 - 0.0333\left(\frac{\phi_1}{100}\right) + 0.333\left(\frac{\phi_1}{100}\right)^2}{\sigma^{0.9625-0.17\left(\frac{\phi_1}{100}\right)-0.85\left(\frac{\phi_1}{100}\right)^3}}$$

Correction factor K_{sh} is the same as described above. $K_{t\delta}$ is the thickness correction for δ^* and can be calculated from the empirical equation given below [2] [3]. This model is based on the design chart from Johnsen and Bullock [6],

$$K_{t\delta} = \frac{6.25 t_{max}}{C} + 37.5 \left(\frac{t_{max}}{C}\right)^2$$

2.3.4 Rotor Blade Angles

As the blade angles have not been specified in Yan et al. [1], an accurate prediction for these values should be calculated. These angles must also reflect the design requirements from Table 3.1. This methodology of determining blade angles and blade geometry from design/near optimum gas incidence and deviation angles can be adopted from Aungier's [2] procedure for blade design.

1. Once the relative flow angles are calculated, start with the assumption that the blade angles are equal to the relative flow angles. ($\beta_1 = \phi_1,\ \beta_2 = \phi_2$)
2. With the design value of blade solidity (σ) and the camber angle estimation,$\theta_{est} = \beta_1 - \beta_2$ proceed with the design incidence angle and design deviation models (equations 2.7-2.14).
3. Use the values δ^* and i^* to calculate the new values for the blade metal angles.

$$\beta_1 = \phi_1 - i^*, \beta_2 = \phi_2 - \delta^*$$

4. Iterate till the blade camber angle θ converges.

2.3.5 Stator Blade Angles

The same procedure has to be followed for the stator angle predictions. But the flow angles for the stator blade passages are as follows,

$$\alpha_{1s} = \alpha_2(rotor),\ \alpha_{2s} = \alpha_1(rotor) \qquad 2.15$$

Then the solution technique is started with equation 2.16; replace all the relative flow angles with the stator absolute angles while calculating the design incidence and design deviation angles. Refer to Table 3.3 for the results.

$$\beta_1 = \alpha_{1s},\ \beta_2 = \alpha_{2s} \qquad 2.16$$

2.3.6 Inlet Guide Vane Design

The blade profile chosen for the IGV is NACA A4K6 63-series. This profile has excellent flow guidance and a wide incidence operating range. Maximum thickness of this blade is at 35% of chord and location of the maximum camber is at 37.5% of chord [2]. Lieblein's model for design incidence angle can be applied to blades with a/C = 0.5 only. In order to treat blades with a different location of maximum camber the following procedure can be adopted [2].

Table 2-3: Blade Geometry

ROTOR			**STATOR**	
Parameter	*Value in degrees.*		*Parameter*	*Value in degrees.*
ϕ_1	61.95			
ϕ_2	51.55		α_1	35.02
α_1	4.76		α_2	4.76
α_2	35.02		β_1	32.79
β_1	60.32		β_2	-1.99
β_2	45.61		θ	34.78
θ	14.70		λ	18.12
λ	53.45		α^*_{AOA}	14.87
α^*_{AOA}	8.50		i^*	0.20
i^*	1.63		δ^*	6.75
δ^*	5.93			

1. Change the sign of all angles ($\Phi_1, \Phi_2, \beta_1, \beta_2\ and\ \lambda$) since the equations 2.7-2.14 are based on blades which have positive turning or camber; inlet guide vanes have negative camber.
2. Compute a pseudo incidence angle ($\bar{\imath}^*$) from equation 2.11.
3. Compute a pseudo angle of attack ($\bar{\alpha}^*_{AOA}$) from equation 2.8 to calculate an initial value for the stagger angle.
4. Adjust the design angle of attack by,

$$\alpha^*_{AOA} = \bar{\imath}^* + \frac{a\theta}{C}$$

Then the actual incidence is given by equation 2.12.

5. Design deviation angle for the inlet guide vanes is a modified form of the Howell's correlation [11]. Lieblein's model includes correction factors for thickness-to- chord ratio and profile shape effects to the Howell's model [3].

$$\delta^* = \frac{0.92\left(\frac{a}{c}\right)^2 + 0.002\beta_2}{1 - 0.002\theta/\sqrt{\sigma}}\frac{\theta}{\sqrt{\sigma}} + \left(K_{sh}K_{t_\delta} - 1\right)(\delta^*_0)_{10} \qquad 2.17$$

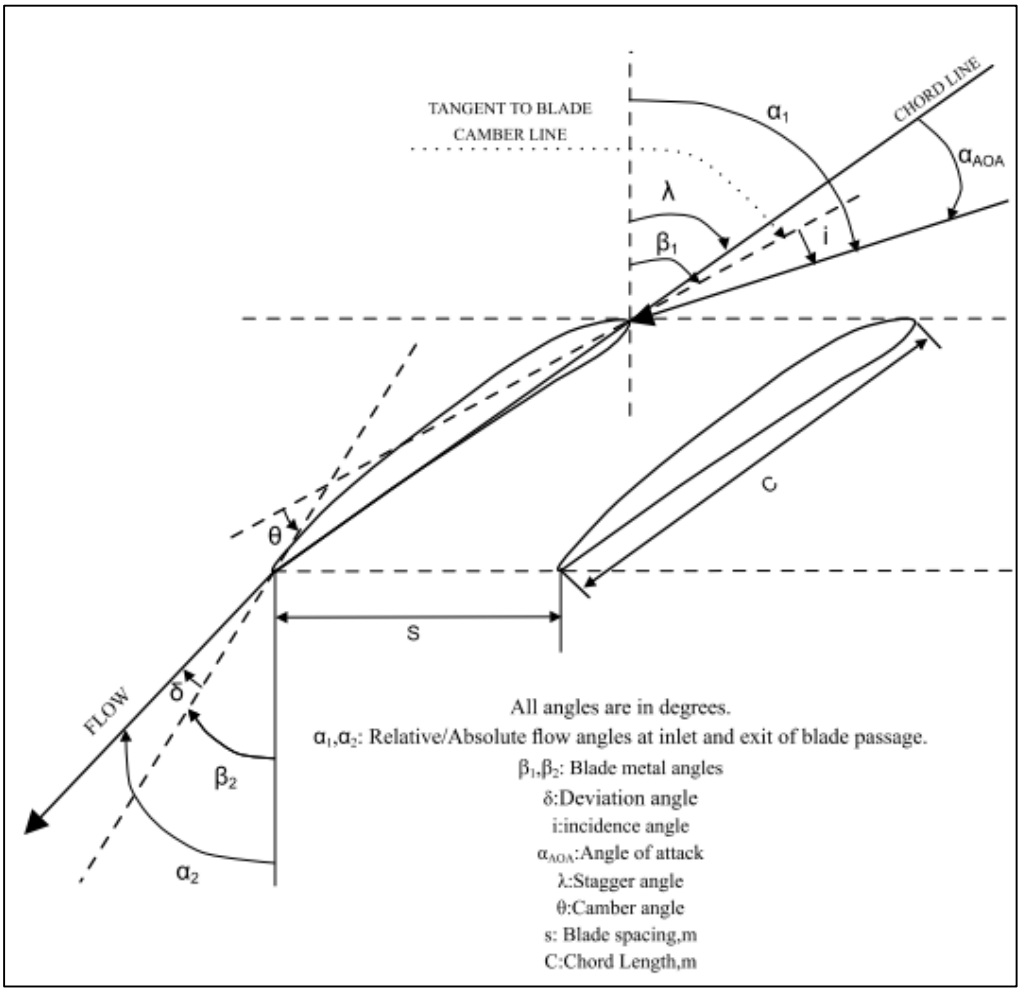

Figure 2-3: Compressor blade nomenclature

6. Compute the new blade angles from these values of design deviation and incidence angles.
7. Iterate till camber angle θ converges.
8. Change the signs of all angles to satisfy the sign convention. Refer to Table 2-4 for results.

Table 2-4: Inlet Guide Vane Design

INLET GUIDE VANE

Parameter	Value in degrees
α_1	0.00
α_2	4.76
β_1	12.96
β_2	3.71
θ	-9.24
λ	-3.17
i^*	-12.96
δ^*	1.04

Chapter 3

Loss Models

An ideal compressor is a machine which isentropically compresses the working fluid from total conditions T_{01}, P_{01} to exit total conditions $T_{02,s}$ and $P_{02,s}$. But a real compressor is one which compresses the working fluid from T_{01}, P_{01} to exit conditions T_{02} and P_{02} with added losses. In this chapter, the losses that affect the work done on the fluid will be analyzed.

The losses are categorized as [5],

1. Group I Losses:

This category includes the pressure losses caused by boundary-layer friction on the primary flow [blade passages] as well as the secondary flow [end wall, hub to stator clearance] . The other types of losses in this category are the leakage or clearance losses.

2. Group II Losses:

Losses associated with friction caused by a rotating disk on the fluid can be grouped as windage or mechanical losses. These losses increase the enthalpy across a rotating blade passage by consuming a small fraction of the shaft work.

The disk friction is predominant in small turbomachines operating at a very low Reynold's number. Hence the windage loss effects are neglected in the current analysis.

However for low Reynold's number operation of small turbomachines the windage losses can be calculated as follows [12],

$$W_C^{\dot{d}ısk} = 3.75 \exp(-3)\, \rho_i D^2 U^3$$

The pressure loss coefficient can be written as [14],

$$Y = Y_p + Y_{TC}$$

3.1 Profile Loss Coefficient, Y_P

Lieblein [13] had shown that the losses associated with a blade passage are a function of a boundary-layer "momentum" thickness, $\theta_{TE,}$ at the trailing edge. This boundary-layer momentum thickness is primarily influenced by the blade surface velocity distributions and surface skin friction. Thus the amount of deceleration caused on the blade surface can be used to determine the momentum thickness [2].

The amount of diffusion can be calculated as [2],

$$D_{eq} \approx \frac{W_{max}}{W_2}$$

Lieblein [3] developed an equivalent diffusion ratio based on 2-D cascade data of the same NACA-65 series to determine the boundary-layer charactersitics at the trailing edge [13]. However, Koch and Smith[15] added correction factors to this diffusion ratio based on cascade data to account for highlly turbulent boundary layers.

$$\begin{aligned} D_{eq} &\equiv \frac{W_1}{W_2}\left[1 + 0.7688\left(\frac{t_{mx}}{c}\right) + 0.6024\Gamma\right] \\ &\times \left\{(\sin\alpha_1 - 0.2445\sigma\Gamma)^2 \right. \\ &\left. + \left(\frac{\cos\alpha_1}{1 - \left[0.4458\sigma(t_{max}/c)/\cos\left((\alpha_1 + \alpha_2)/2\right)\right][1 - [1 - (A_2/A_1)]/3]}\right)^2\right\}^{1/2} \end{aligned} \quad 3.1$$

The circulation term, Γ is given by[14],

$$\Gamma = \frac{r_{1m}V_1 sin\alpha_1 + r_{2m}V_2 sin\alpha_2}{\frac{r_{1m} + r_{2m}}{2} W_1\sigma}$$

Koch and Smith [15] developed models for the boundary layer momentum thickness and shape factor based on their experimental data. The nominal conditions being,

- No contraction of the flow annulus height, h;
- An inlet Reynolds number of $Re_1 = \rho_1 W_1 C / \mu_1 = 10^6$

- Hydraulically smooth blades.

The momentum thickness is given as [15],

$$\frac{\theta_2^o}{C}(nominal) = \left[0.0072 \times D_{eq} - 0.0032\right] \times \left[1.0 \times 0.2234 \times \left(D_{eq} - 1.0\right)^6\right] \quad 3.2$$

For flow condtions other than nominal, correction factors were also introduced by the same investigator,

$$\frac{\theta_2}{C} = \left(\frac{\theta_2^o}{C}\right) \times \zeta_M \times \zeta_H \times \zeta_{Re} \quad 3.3$$

Where,

$$\zeta_M = 1.0 + \left(0.117569 - 0.169832 \times D_{eq}\right) \times Ma_1^n$$

$$n = 2.8532 + D_{eq} \times \left(-0.977474 + 0.194771 \times D_{eq}\right)$$

$$\zeta_H = 0.53\frac{H_1}{H_2} + 0.47$$

$$\zeta_{Re} = \begin{cases} \left(\frac{10^6}{Re_1}\right)^{0.166}, & Re_1 \geq 2 \times 10^5 \\ 1.30626 \times \left(\frac{2 \times 10^5}{Re_1}\right)^{0.5}, & Re_1 < 2 \times 10^5 \end{cases}$$

The shape facter for the trailing edge is given as [15],

$$H_{TE}^o(nominal) = \frac{\delta_{TE}^*}{\theta_2^o} = 1.231 + D_{eq}^3 \times \left(0.0476 + 0.00207 \times {D_{eq}}^6\right) \quad 3.4$$

For other conditions,

$$H_{TE} = H_{TE}^o \times \xi_M \times \xi_H \times \xi_{Re} \quad 3.5$$

Where,

$$\xi_M = 1.0 + \left[1.07247 + D_{eq} \times \left(-0.867098 + 1.80425 \times D_{eq}\right)\right] \times Ma_1^{1.8}$$

$$\xi_H = 1.0 + \left[\frac{H_1}{H_2} - 1.0\right] \times \left(0.0026 \times {D_{eq}}^8 - 0.024\right)$$

$$\xi_{Re} = \left(\frac{10^6}{Re_1}\right)^{0.06}$$

Thus the profile loss coefficient can be calculated as [5],

$$Y_p = \frac{\Delta \dot{P}_{loss}}{\rho_1 \frac{W_1^{\ 2}}{2}} = 2\left(\frac{\theta_2}{C}\right) \times \frac{C}{S\cos\phi_2} \times \left(\frac{\cos\phi_1}{\cos\phi_2}\right)^2 \times \left(\frac{2H_{TE}}{3H_{TE}-1}\right) \times \left[1 - \left(\frac{\theta_2}{C}\right)\frac{C}{S}\frac{H_{TE}}{\cos\phi_2}\right]^{-3} \quad 3.6$$

3.2 Leakage Loss Coefficient, Y_{TC}

As the compressor operates with some clearance between the tips of the rotor blades and the casing as well as some clearance between the tips of stator and hub, a fraction of the fluid leaks across these blade tips. This affects the work done on the fluid by the compressor. The leakage loss can be defined as [14],

$$Y_{TC} = Y_{tip} + Y_{gap} \quad 3.7$$

Where,

$$Y_{tip} = 1.4K_e \frac{C}{S} \times \frac{\tau}{H} \times \left(\frac{\cos\phi_2}{\cos\phi_m}\right)^2 \times C_L^{1.5}$$

$$\phi_m = \tan^{-1}\left[\frac{1}{2}[\tan\phi_1 - \tan\phi_2]\right]$$

And,

$$Y_{gap} = 0.0049K_G \frac{C}{S} \times \frac{C}{H} \times \frac{\sqrt{C_L}}{\cos\phi_m}$$

$$C_L = 2\frac{S}{C} \times \cos\phi_m \times [\tan\phi_1 + \tan\phi_2]$$

$$K_e = \begin{cases} 0.5 \; for \; mid-loaded \; blades \\ 0.566 \; for \; front \; or \; aft \; loaded \; blades \end{cases}, K_G = \begin{cases} 1.0 \; for \; mid-loaded \; blades \\ 0.943 \; for \; front \; or \; aft \; loaded \; blades \end{cases}$$

3.3 Incidence Angle Correction Factor, K_{inc}

To compute the pressure loss coefficient during off design operation, Aungier [2] has developed a correction factor for the pressure loss coefficient

$$Y = K_{inc}[Y_p + Y_{TC}] \tag{3.8}$$

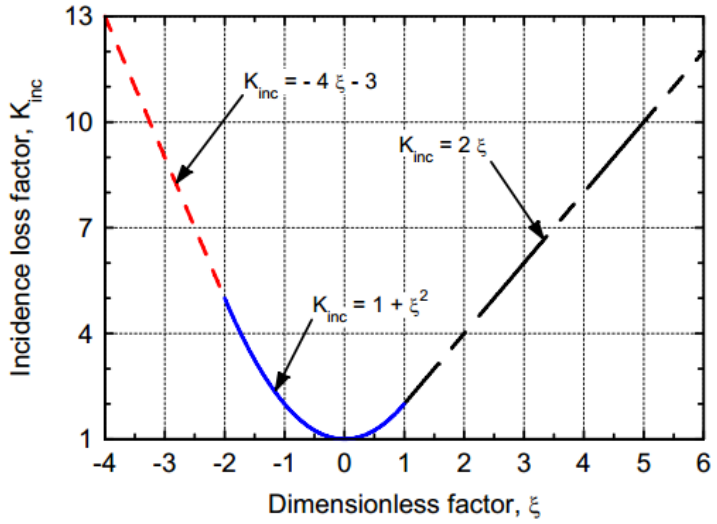

Figure 3-1 Incidence Angle Correction Factor [14]

The correction factor is computed by establishing the positive stall incidence angles and the negative stall incidence angles. Aungier [2] states that the incidence angle has significant influence on the pressure loss coefficient, Y. At the positive and negative stall incidence angles the loss coefficient is twice the minimum pressure loss coeffcient. Refer to Figure 3-2.

$$i_s = i^* + 10.3 + \frac{\left(2.92 - \frac{\phi_1}{15.6}\right)\theta}{8.2} \tag{3.9}$$

$$i_c = i^* - 9.0 + \frac{\left(1.0 - \left(\frac{30}{\phi_1}\right)^{0.48}\right)\theta}{4.176} \tag{3.10}$$

The optimum incidence angle is computed using the relations from chapter 3; equation 3.12.

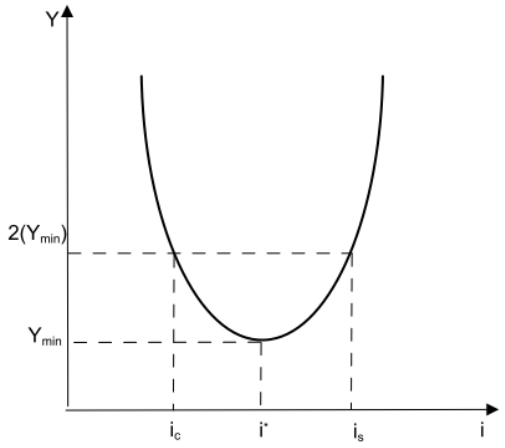

Figure 3-2 Incidence Angle Loss Bucket

It is clear from the Figure 4-1 that [2],

$$K_{inc} = \begin{cases} [-4\xi - 3], & if\ \xi < -2 \\ [1 + \xi^2], & if\ -2 \leq \xi \leq 1 \\ 2\xi, & if\ \xi > 1 \end{cases}$$

The normalized incidence angle parameter, ξ can be defined as,

$$\xi = \begin{cases} \dfrac{i - i^*}{i_s - i^*}\ when\ i \geq i^* \\ \dfrac{i - i^*}{i^* - i_C}\ when\ i < i^* \end{cases}$$

Chapter 4

Two-Dimensional Incompressible Flow Analysis

The solution technique will be described in this chapter. Each stage is divided into four sections.

- Stator Leading Edge (isentropic contraction zone) [0-1]
- Stator Cascade(leading edge to trailing edge with added profile losses) [1-2]
- Rotor Leading Edge(isentropic contraction zone) [0-1]
- Rotor Cascade(leading edge to trailing edge with added profile losses) [1-2]

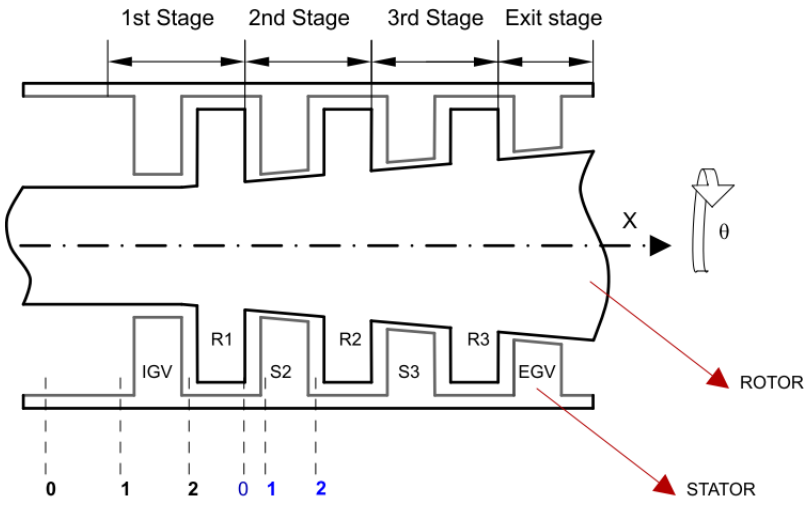

Figure 4-1: A Typical Multistage Axial Compressor

The incompressible flow formulations used in this chapter are justifiable as the maximum Mach number throughout the compressor is 0.1-0.3. The difference in the formulations will be due to the presence of density terms in the total pressure formulation.

$$P_0 = P\left[1 + \frac{M^2}{2\left(\frac{C_p}{R} - 1\right)}\right]^{\frac{C_p}{R}} \approx P + \frac{V^2}{2}\rho_0 \; [incompressible\ Bernoulli\ formulation]$$

This equation is valid for flows with a Mach number of upto 0.4, with an error percent of 1.0 and at higher Mach numbers (upto 0.6) the error percent is still less than 2.5 [5].

4.1 Stator Cascade [1-2] Methodology

This method is adopted from literature [14] with some necessary modifications to account for the off-design deviation angle consideration. With the known values at station 1 we can compute the cascade performance of a stator blade as depicted in Figure. 4-2 with the help of the following equations. Start with an assumption for the absolute gas flow ange at the trailing edge; assume deviation angle is zero and loss coefficient is 0.

The effects of convective and radiative heat transfer losses are neglected in the current analysis.

$\alpha_2 = \beta_2 . + \delta$

$$\dot{m} = \rho_2 V_2 A_2 \cos(\alpha_2) \tag{4.1}$$

$$\dot{m} h_{t1} = \dot{m}\left(h_2 + \frac{1}{2}V_2^2\right) \tag{4.2}$$

$$P_{t1} = P_2 + \left(\frac{1}{2}\rho_2 V_2^2\right) + \Delta P_{loss} \tag{4.3}$$

These three conservation equations can be used to solve the velocity polynomial as,

$$V_2 = \frac{-B - (B^2 - 4AC)^{0.5}}{2A} \tag{4.4}$$

$$A = \frac{\frac{1}{2}\dot{m}}{A_2 \cos(\alpha_2)}\left(1 - \frac{RZ_2}{C_p}\right), B = -P_{t1} + \Delta P_{loss}$$

$$C = \frac{z_2 \dot{m}}{A_2 \cos(\alpha_2)} R \left(\frac{h_{t1}}{C_p} - T_{ref} \right)$$

Refer to Appendix-B for the velocity polynomial derivation.

Where,

$$\Delta P_{loss} = \frac{Y \rho_1 V_1^2}{2}$$

Using equation 4.1 and 4.2 we can find the values of density and temperature. With an initial guess for the compressibility term Z_2, the gas pressure can be calculated as

$$P_2 = \rho_2 R Z_2 T_2 \qquad 4.5$$

And the deviation angle is [2],

$$\delta = \delta^* + \left[\frac{\partial \delta}{\partial i}\right]^* (i - i^*) + 10(1 - W_{2X}/W_{1X}) \qquad 4.6$$

Where $\left[\frac{\partial \delta}{\partial i}\right]$ is the term which accounts for the difference in the incidence angle at off-design conditions.

$$\left[\frac{\partial \delta}{\partial i}\right]^* = [1 + (\sigma + 0.25\sigma^4)(\phi_1/53)^{2.5}]/exp(3.1\sigma)$$

$$\alpha_2 = \beta_2 + \delta \qquad 4.7$$

$Z_2 = f(T_2, P_2)$, refer to Appendix-A

Calculate the pressure loss coefficient, Y and update the values of absolute gas angle and the compressibility factor, Z for the next iteration. Repeat the steps untill convergence is achieved on the deviation angle.

The solution technique for the stator leading edge zone is the same as above with the subscripts 1-2 replaced by 0-1. In this zone Y = 0(isentropic flow assumption) and,

$$i = \alpha_1 - \beta_1 \qquad 4.8$$

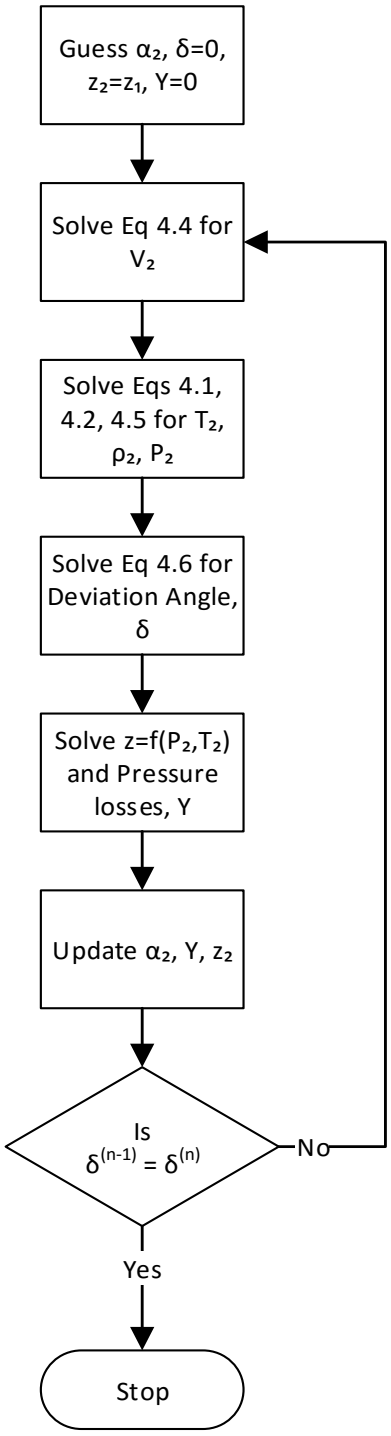

Figure 4-2: Stator Cascade [1-2] Methodology

4.2 Rotor Cascade Methodology

As shaft work is being done on this blade passage, the solution technique described above cannot be used for the rotor cascade. The momentum balance equation is,

$$P_1 + \frac{\rho_1 W_1^2}{2} - \Delta P_{loss} = P_2 + \frac{\rho_2 W_2^2}{2} \tag{4.9}$$

The pressure loss is defined as,

$$\Delta P_{loss} = \frac{Y \rho_1 W_1^2}{2}$$

$$P_1 + \frac{\rho_1 W_1^2}{2}(1 - Y) - P_2 - \frac{\rho_2 W_2^2}{2} = 0 \tag{4.10}$$

$$\phi_2 = \beta_2 + \delta \tag{4.11}$$

All the parameters at station 2 in equation 4.10 can be expressed in terms of W_2 using the following velocity triangle realtions and conservation equations [14]. Assume deviation angle is equal to 0 and set pressure loss coefficient term, Y to 0.

$$V_2 = (W_2^2 - 2U_2 W_2 \sin\phi_2 + U_2^2)^{1/2} \tag{4.12}$$

$$\tan\alpha_2 = \frac{U_2/W_2 - \sin\phi_2}{\cos\phi_2} \tag{4.13}$$

$$\rho_2 = \frac{\dot{m}}{A_2 V_2 \cos\alpha_2} \tag{4.14}$$

The Euler equation is given as,

$$\dot{W}_c = \dot{m} \times (U_1 V_{1\theta} - U_2 V_2 \sin\alpha_2) \tag{4.15}$$

Gas Temperature can be calculated from the energy equation.

$$T_2 = T_1 + \frac{V_1^2 - V_2^2}{2C_p} - \frac{\dot{W}_c}{\dot{m} C_p} \tag{4.16}$$

$$P_2 = \rho_2 R T_2 Z_2 \tag{4.17}$$

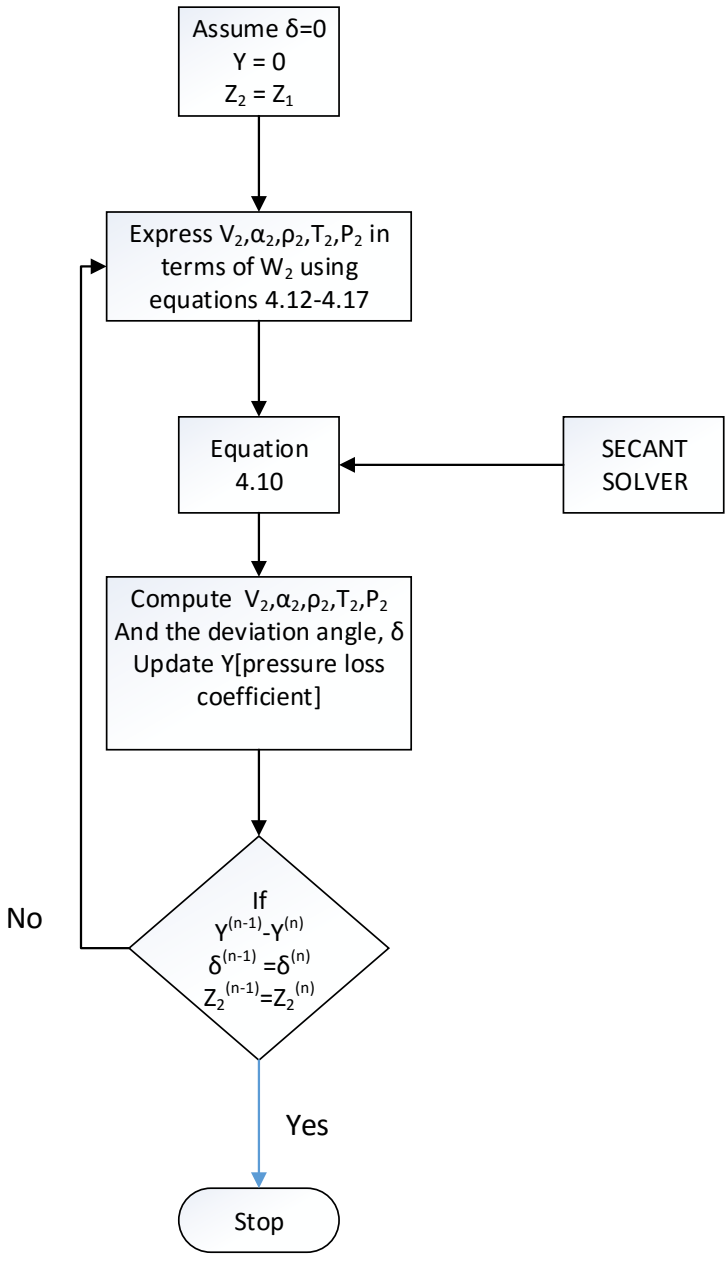

Figure 4-3: Rotor Cascade Methodology

By expressing all these quantities in terms of W_2, we can solve for the correct W_2 by performing a simple Secant root solving technique on equation 5.10. Once the correct

relative velocity at the trailing edge has been calculated, re-compute Z_2 , deviation angle and pressure loss coefficient till convergence is achieved on these quantities.

The rotor leading edge section [0-1] is analyzed in the same way as the stator leading edge. The incidence angle and relative gas velocity at the leading edge are calculated as follows [14],

$$W_{1x} = V_1 \cos(\alpha_1)$$
$$W_{1\theta} = V_1 \sin(\alpha_1) - U_1$$
$$W_1 = \sqrt{(W_{1x}^2 + W_{1\theta}^2)}$$
$$\phi_1 = \tan^{-1}(-W_{1\theta}/W_{1x})$$
$$i = \phi_1 - \beta_1$$

Chapter 5

Results

5.1 Validation

This chapter includes the results of the analytical model developed in this research and is validated with experimental and computational results in Yan et al. [1]. The prediction-charts of the 4-stage and 20-stage compressors in Ref. [1] are developed using the FORTRAN program for further performance analysis.

As compressor performance is highly influenced by inlet conditions, a series of tests were performed on the 4-stage compressor by Yan [1]. CASE 1 & CASE 2 corresponds to different sets of airfoils. The different inlet conditions are identified by the Run number. Data are provided for only three such tests [1].

Table 5-1: Test Compressor Inlet Conditions

CASE # RUN #	$\mathbf{T_{in}}$ [K]	$\mathbf{P_{in}}$ [MPa]
CASE 1 RUN 12	303.85	0.896
CASE 1 RUN 9	285.85	0.200
CASE 1 RUN 7	300.65	0.543

The simulated results(Table 5.2) are in good agreement with the experimental data with an error percentage less than 2.5% for the static conditions and 6-7% for the efficiencies. This difference in calculated data and measured data can be attributed to the following reasons,

1. The airfoils used in the experimental compressor are a type of subsonic controlled diffusion airfoils.The design goals of this airfoil “includes adjusting incidence to achieve single stagnation point near the leading edge, limiting peak Mach number

on the suction surface, and achieving suction surface diffusion from the peak Mach number until the trailing edge without separation." [1]

Table 5-2: Comparison of Simulation Results with Benchmarked CFD Results and Experimental Data

Parameter	Mass Flow Rate= 12.47 kg/s			Mass Flow Rate = 12.42 kg/s		
	Experimental	Analytical	%err	CFD	Analytical	%err
P_{0e} , MPa	1.049	1.0451	0.37	1.049	1.046	0.26
P_{ex}/P_{in}	1.168	1.146	1.90	1.166	1.147	1.59
Exit T_t , K	325.56	328.50	0.90	325.37	328.74	1.03
η_e	0.884	0.817	7.57	0.874	0.818	6.42

2. The loss models used in the program are formulated from the cascade data of air compressors, refer to Chapter 3. Due to the lack of sufficient cascade data for helium compressors, the loss models used in this research are for air compressors and not helium compressors.
3. The polytropic efficiency is highly sensitive towards the total pressure and temperature change across the compressor. It is given by the formula,

$$\eta_p = \frac{\gamma - 1}{\gamma} \frac{\ln\left(\frac{P_{0\,ex}}{P_{0\,in}}\right)}{\ln\left(\frac{T_{0\,ex}}{T_{0\,in}}\right)}$$

The analytical results are validated using the experimental results in [1] in the subsequent graphs.

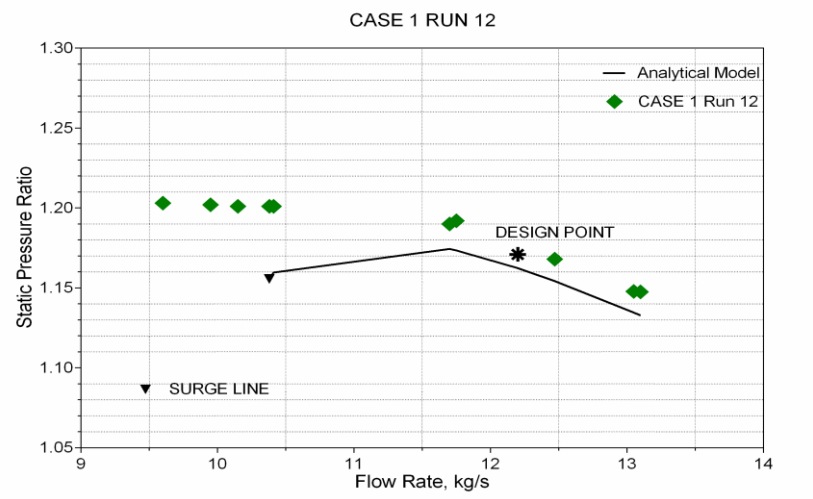

Figure 5-1: Measured and Calculated Pressure Ratio for CASE 1 RUN 12

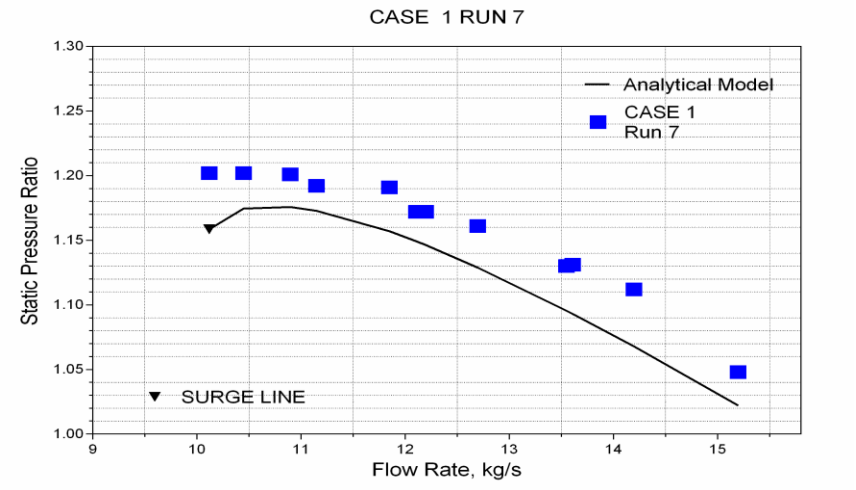

Figure 5-2: Measured and Calculated Pressure Ratio for CASE 1 RUN 7

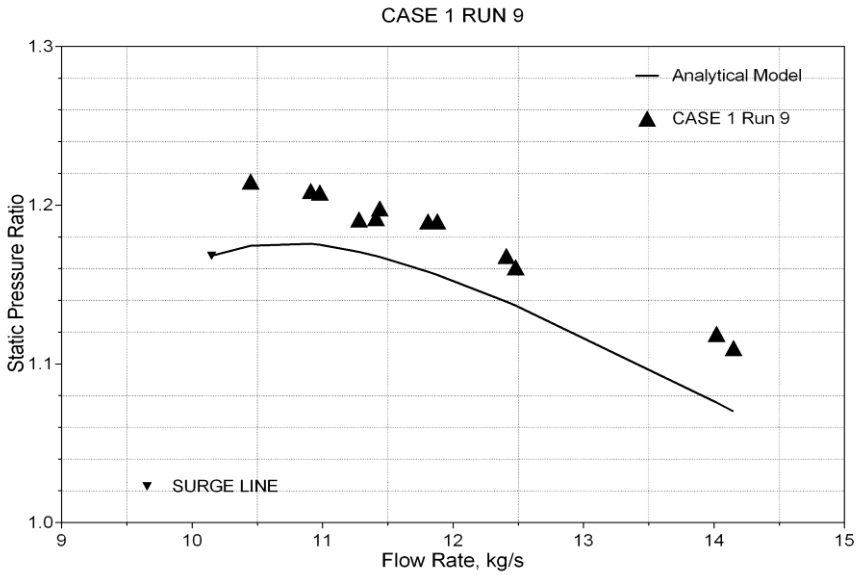

Figure 5-3: Measured and Calculated Values for CASE 1 RUN 9

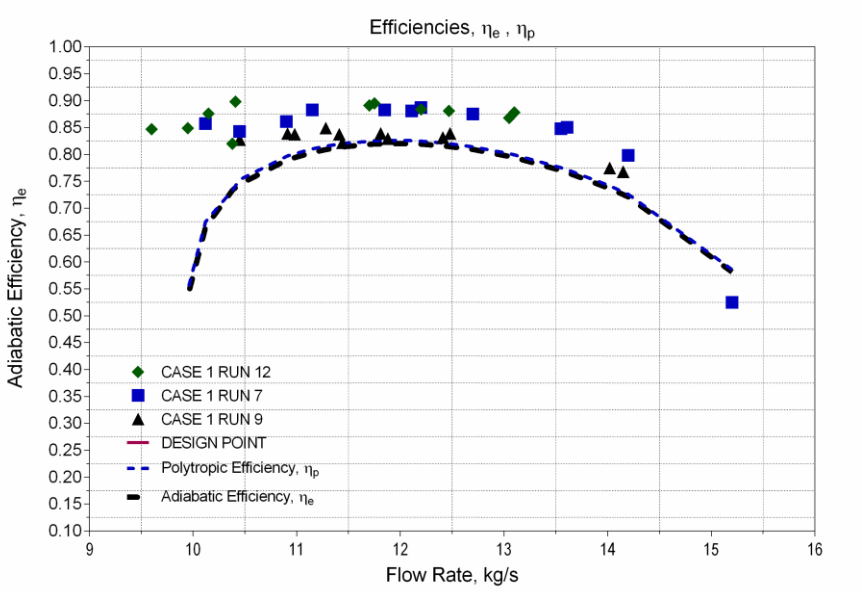

Figure 5-4: Measured and Calculated Values for Adiabatic Efficiency and Polytropic Efficiency

5.2 Prediction-Charts for 4-Stage Test Compressor

The performance maps are generated for the test compressor operating at nominal inlet conditions and speed. The nominal inlet conditions are

- T_{in} = 303.15 K
- P_{in} = 0.883 MPa
- N = 10800 RPM

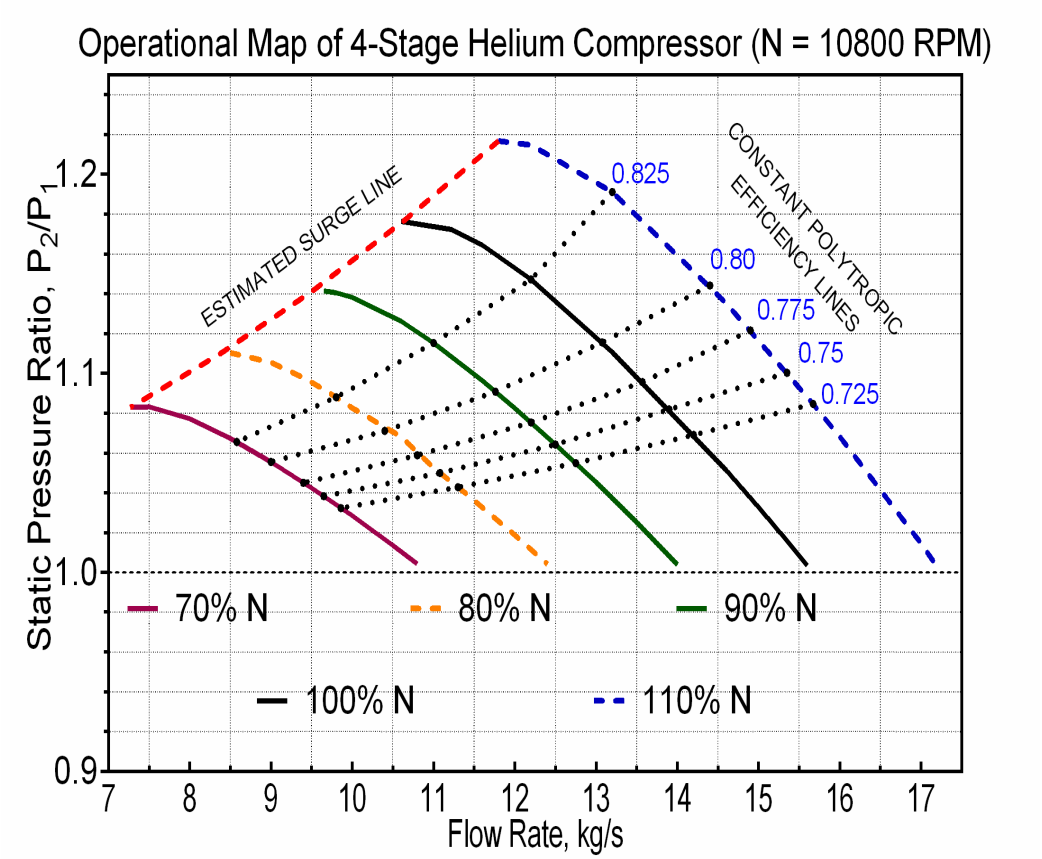

Figure 5-5: Operational Map of 4-Stage Test Compressor

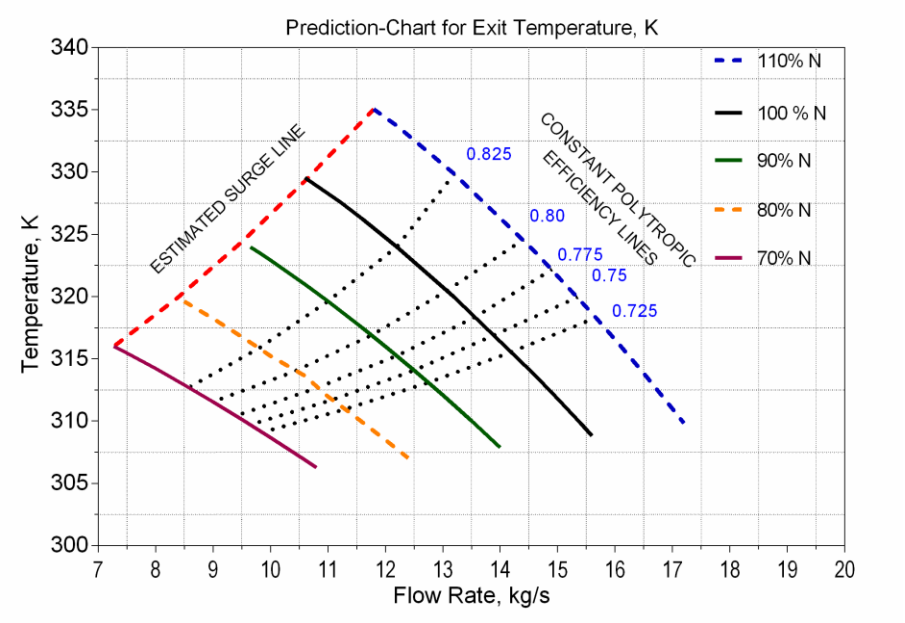

Figure 5-6: Prediction-Chart for Exit Temperature, K

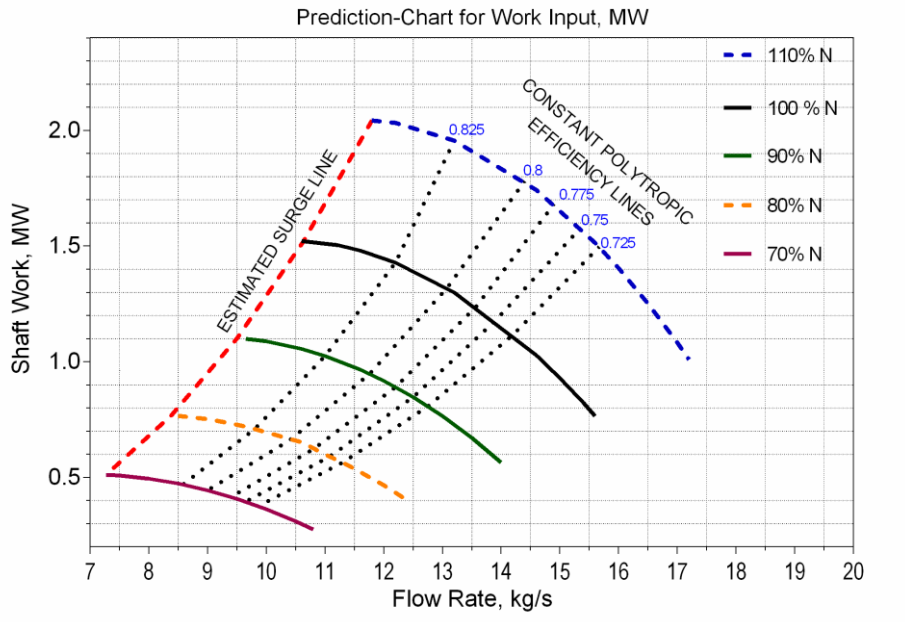

Figure 5-7: Prediction-Chart for Work Input, MW

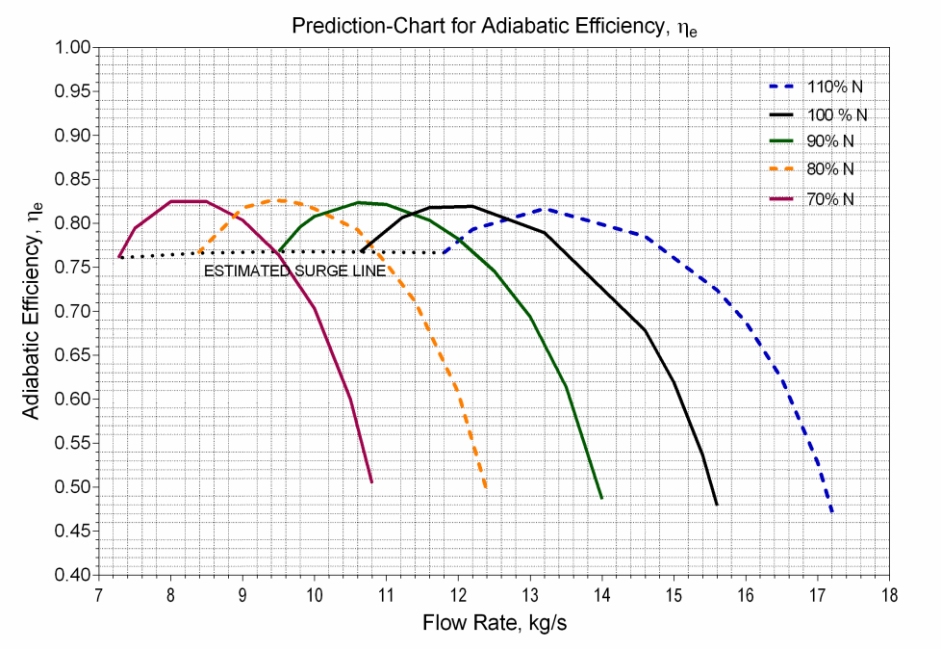

Figure 5-8: Prediction-Chart for Adiabatic Efficiency

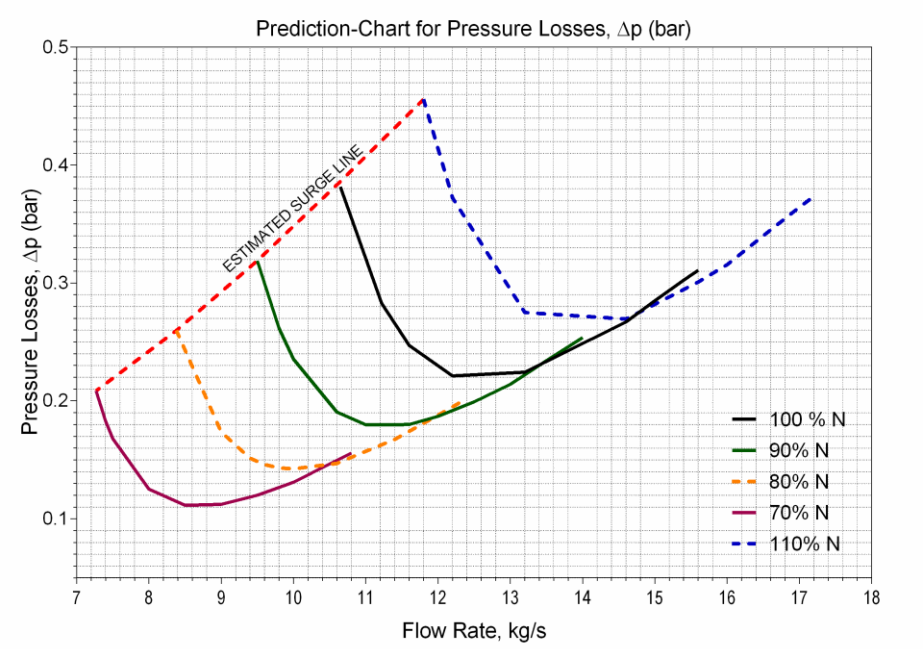

Figure 5-9: Prediction-Chart for Pressure Losses (bar)

5.2.1 Incidence Angle and Pressure Loss Coefficient

This section includes the variation of incidence angle across the compressor and the pressure loss coefficient.

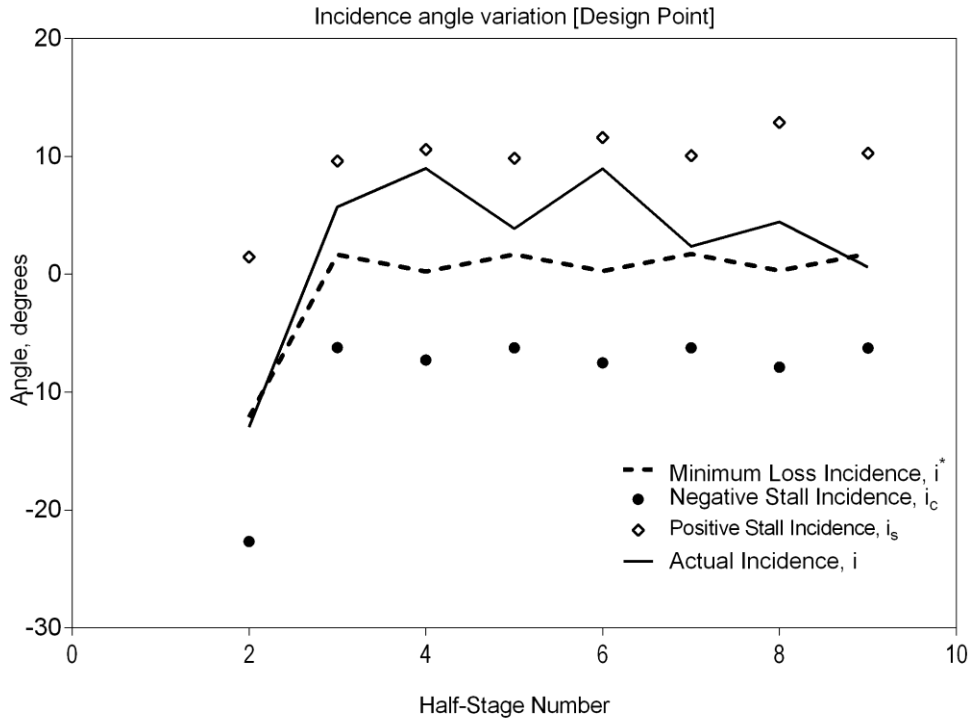

Figure 5-10: Design Incidence Angle and Actual Incidence Angle

The procedure for calculating these angles are described in chapters 2 and 4. Any incidence close to the design incidence does not affect the pressure loss to significant levels [2]. But at values close to the positive stall incidence angles and negative incidence angles the pressure loss coefficient is twice the minimum loss coefficient.

The positive stall incidence occurs due to decrease in mass flow rate and usually appears on the suction side. It also depicts the on set of compressor surge. The negative stall occurs due to choking operation of the compressor and appears at the pressure side

of the blade. The variation of the incidence angle correction factor at off-design conditions is shown in the following charts,

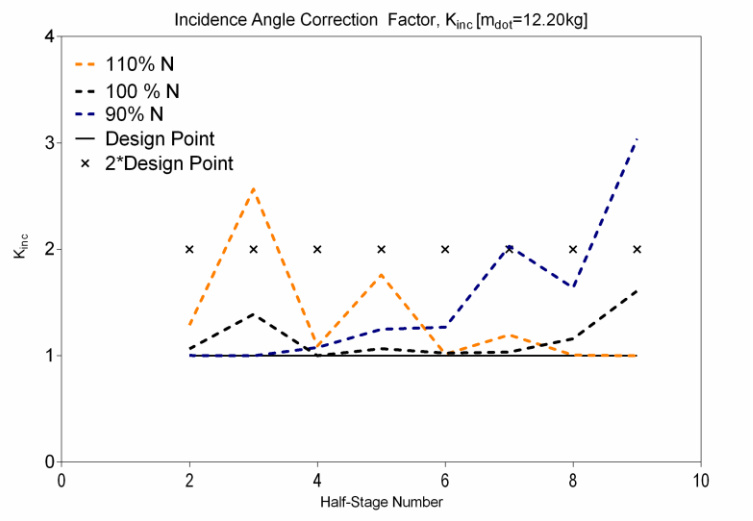

Figure 5-11: Incidence Angle Correction Factor at Off Design Speeds

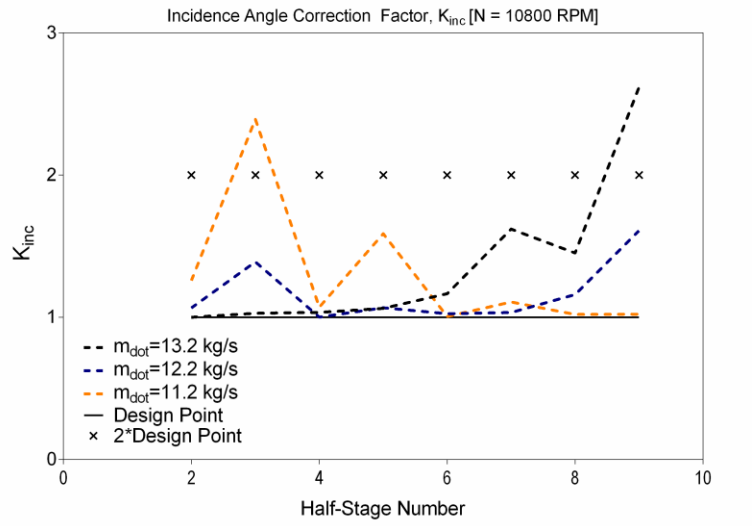

Figure 5-12: Incidence Angle Correction Factor at Off-Design Flow Rates.

5.2.2 Surge Line Prediction

The onset of compressor surge is predicted by these following criteria [2],

1. When the pressure ratio versus mass flow rate goes through a slope of zero with decrease in mass flow rate.
2. The De-Haller number is reached.

$$\frac{W_2}{W_1} < 0.72$$

The De-haller number is very effective in prediciting the stall operation which ultimately leads to compressor surge though it actually identifies the end-wall stall rather than blade stall [2]. The equivalent velocity ratios and their variations during off-design operation is shown below,

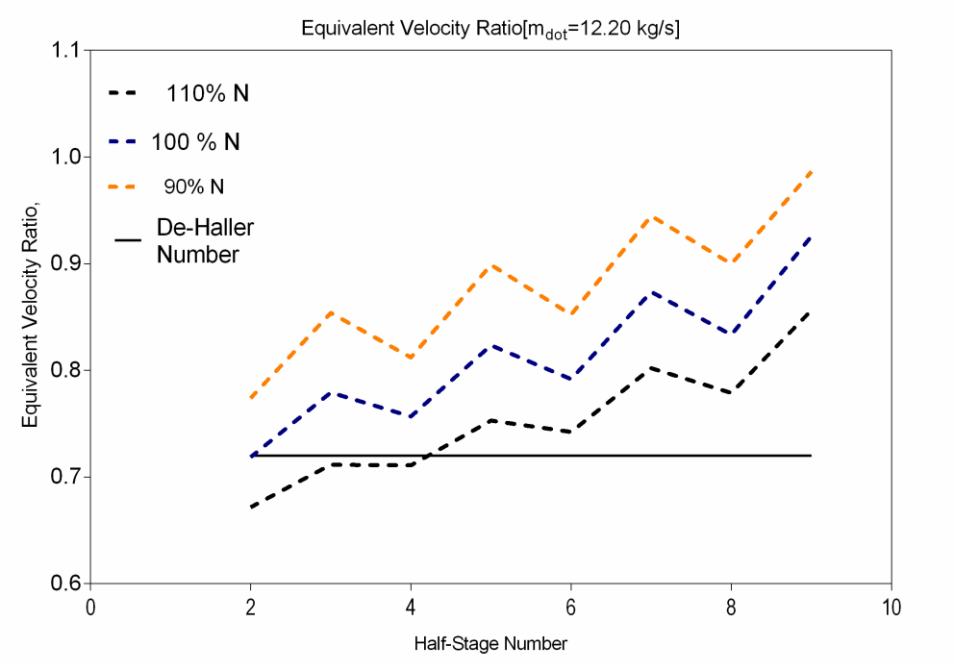

Figure 5-13: Equivalent Velocity Ratios at Off-Design Mass Flow Speeds

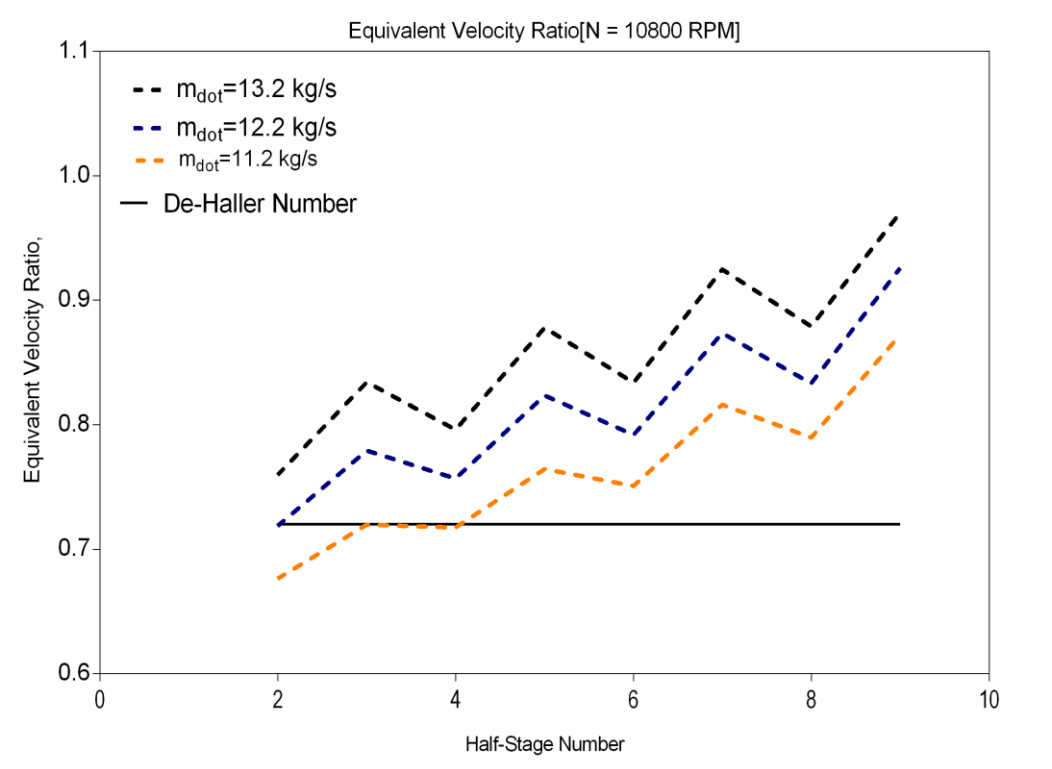

Figure 5-14: Equivalent Velocity Ratio at Off-Design Mass Flow Rates

5.2.3 Deviation Angle (δ) Variations

The deviation angle is calculated using equation 4.6 and the design deviation angle is calculated in chapter 2. These angles are shown in the following charts.

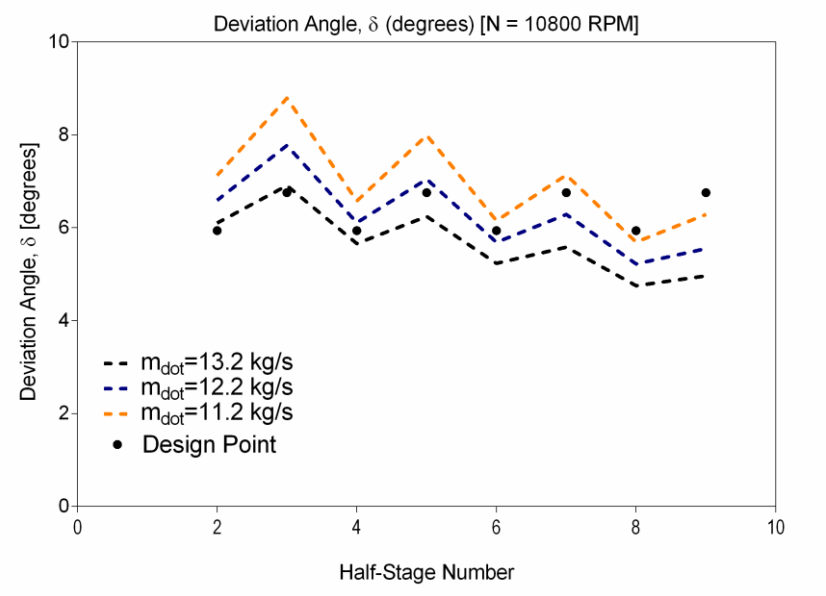

Figure 5-15: Deviation Angle at Off-Design Mass Flow Rates

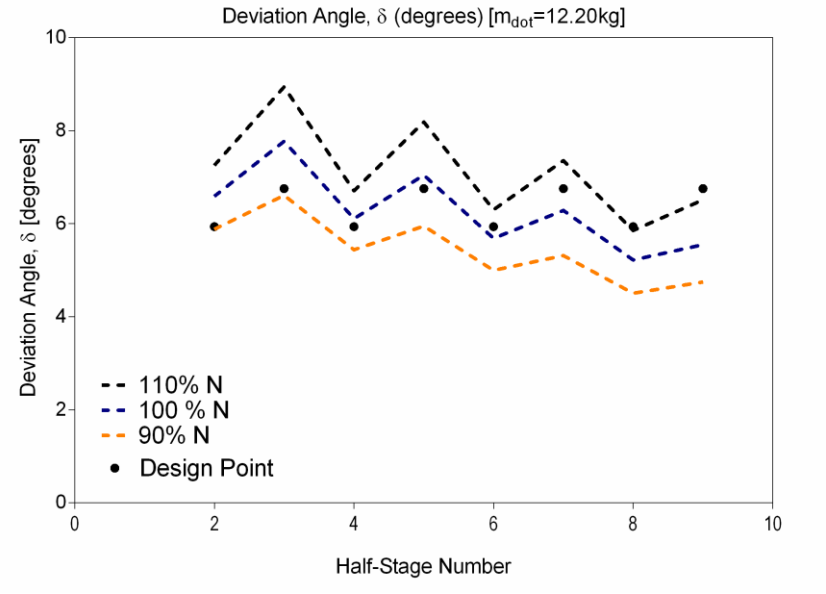

Figure 5-16: Deviation Angle at Off-Design Speeds

5.3 20-Stage Helium Compressor

The same FORTRAN program is used to analyze the full scale helium compressor for the geometry provided in Table 3-1. This compressor is a 20-stage axial compressor and is coupled with the 6-stage helium turbine. The resulting helium gas turbine is rated at 300MWe. The results are in good agreement with the targeted design point operation as well as the CFD results by Yan [1].

The nominal inlet conditions are:

- Inlet static pressure: 3.52 MPa
- Inlet static temperature: 301.5 K
- Rotational Speed: 3600 RPM
- Mass flow rate: 442 kg/s

Table 5-3: Comparison with CFD results [1]

Parameter	CFD	Analytical Model	% err
Static Pressure Ratio	2.078	1.971	5.14
Adiabatic Efficiency, η_{ad}	90.3 %	87.79 %	2.779

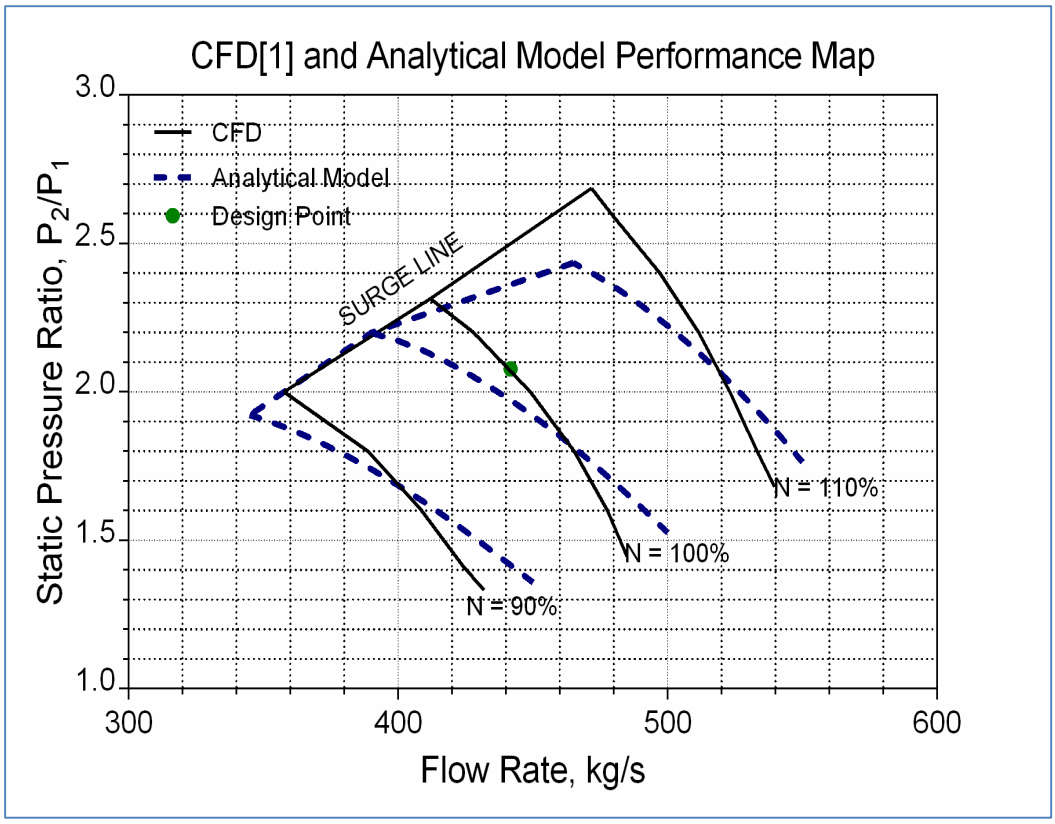

Figure 5-17: Operational Map for CFD [1] and analytical results

Chapter 6

Conclusion and Recommendations

This chapter is a summary of the analysis done in this research work; recommendations for further study are also mentioned.

6.1 Conclusion

After validating the model with the experimental results from Yan [1], a set of prediction-charts have been developed. These charts helps to better understand the behavior of important performance parameters during off-design operations.

The model has provisions for increasing the range of mass flow rate to be studied. Currently the program can simulate up to 5 different speed operations [N].

With an average run time of 2 seconds, this model best suits the need to predict different helium compressors' performance at a very short time. To develop the detailed map files provided in chapter 5, an estimate of the stall and choke region should be known. Hence this analytical model can be used for preliminary analysis and to get an idea of the power required from the turbine or motor.

These sets of design point and off-design performance data can also be used to generate helium compressor map files readable by NPSS [Numerical Propulsion Sytem Simulation]

6.2 Recommendations

To further develop the accuracy of this simulation, the following points should be considered,

- Include heat loss effects, as this might have a minor impact on the total temperature rise across a stage and ultimately the efficiency of the compressor.
- Develop an anlytical model to capture the changes of flow properties across the radial direction.

- Use of semi-empirical loss models developed for helium turbomachinery that may be available after further studies by other authors.
- Extend the research to helium turbines in order to determine the operating line of the turbomachines. It also helps to identify the surge margin of the compressor.

APPENDIX A

SUBROUTINE HeThermo

This section describes the calculations of Helium gas properties at every blade station. These formulations are based on the models by Helge Petersen [9]. Petersen formulated semi-empirical models of Helium gas at pressures from 1 to 100 bars and from temperatures 273 k to about 1800 K. This range of pressure and temperature are applicable to helium-cooled atomic reactor design. The compressibility factor, Z present in the gas law for Helium is determined by virial equations of state.

The virial equations are power expansions in terms of volume or pressure respectively. They are obtained experimentally by fitting of the power series to measured isotherm of the gas [9]. The experimental data were documented by Stroud et al. [10]

A.1 Properties of Helium Gas

A.1.1 Compressibility Factor, Z

$$Z = 1 + \frac{0.4446P}{T^{1.2}} \quad \text{A.1}$$

A.1.2 Density, ρ

$$\rho = \frac{48.14P}{T}\left[1 + \frac{0.4446P}{T^{1.2}}\right]^{-1} \frac{kg}{m^3} \quad \text{A.2}$$

A.1.3 Specific Heats

$$C_p = 5195.00 \frac{J}{kg.K}$$

$$C_v = 3117.00 \frac{J}{kg.K}$$

$$\gamma = 1.6667$$

A.1.4 Coefficient of Dynamic Viscosity, μ

$$\mu = 3.674 \times 10^{-7} \times T^{0.7} \frac{kg}{ms} \quad \text{A.3}$$

A.1.5 Coefficient of Thermal Conductivity, k

$$k = 2.682 \times 10^{-3}(1 + 1.123 \times 10^{-3} \times P)T^{[0.71(1-2.10\times10^{-4}\times P)]} \frac{W}{mK} \quad \text{A.4}$$

A.1.6 Prandtl Number, Pr

$$Pr = \frac{0.7117}{1 + 1.123 \times 10^{-3} \times P} T^{-(0.01-1.42\times10^{-4}\times P)} \quad \text{A.5}$$

Note: All pressures are in bar and all temperatures are in Kelvin (K).

APPENDIX B

Velocity Polynomial Derivation

The velocity polynomial is derved from the conservation equations. The momentum equation is,

$$P_{t1} = P_2 + \left(\frac{1}{2}\rho_2 V_2^2\right) + \Delta P_{loss} \quad \text{B.1}$$

$$\dot{m} = \rho_2 V_2 A_2 \cos(\alpha_2) \quad \text{B.2}$$

$$\dot{m} h_{t1} = \dot{m}\left(h_2 + \frac{1}{2}V_2^2\right) + Q_{loss} \quad \text{B.3}$$

Q_{loss} is neglected in the current simulation.

$$P_{t1} - \Delta P_{loss} = z_2 \rho_2 R T_2 + \left(\frac{1}{2}\right) V_2 \times \frac{\dot{m}}{A_2 \cos(\alpha_2)}$$

$$= \frac{z_2 \dot{m}}{A_2 \cos(\alpha_2) V_2} R T_2 + \left(\frac{1}{2}\right) V_2 \times \frac{\dot{m}}{A_2 \cos(\alpha_2)}$$

$$\frac{z_2 \dot{m}}{A_2 \cos(\alpha_2) V_2} R T_2 + \left(\frac{1}{2}\right) V_2 \times \frac{\dot{m}}{A_2 \cos(\alpha_2)} - (P_{t1} - \Delta P_{loss}) V_2 = 0 \quad \text{B.4}$$

From the energy equation B.3, the gas temperature is,

$$T_2 = \frac{h_{t1}}{C_p} - T_{ref} - \frac{\frac{1}{2}V_2^2}{C_p}$$

Substituting this equation for temperature in equation B.4 we have,

$$\frac{z_2 \dot{m}}{A_2 \cos(\alpha_2) V_2} R \left(\frac{h_{t1}}{C_p} - T_{ref} - \frac{\frac{1}{2}V_2^2}{C_p}\right) + \left(\frac{1}{2}\right) V_2 \times \frac{\dot{m}}{A_2 \cos(\alpha_2)} - (P_{t1} - \Delta P_{loss}) V_2 = 0 \quad \text{B.5}$$

The above equation can be reduced to a second order polynomial as follows,

$$A = \frac{\frac{1}{2}\dot{m}}{A_2 \cos(\alpha_2)}\left(1 - \frac{R Z_2}{C_p}\right)$$

$$B = -(P_{t1} - \Delta P_{loss})$$

$$C = \frac{z_2 \dot{m}}{A_2 \cos(\alpha_2)} R \left(\frac{h_{t1}}{C_p} - T_{ref} \right)$$

$$V_2 = \frac{-B - (B^2 - 4AC)^{0.5}}{2A} \qquad \text{B.6}$$

References

[1] Yan, X., Takizuka, T., Kunitomi, K., Itaka, H. and Takahashi, K. (2008).”Aerodynamic Design, Model Test, and CFD Analysis for a Multistage Axial Helium Compressor”. Journal of Turbomachinery, vol. 130(3), 031018.

[2] Aungier, R. H., 2003, Axial-Flow Compressors: A Strategy for Aerodynamic Design and Analysis, ASME Press, New York, NY.

[3] Lieblein, S., 1960, “Incidence and Deviation-Angle Correlations for Compressor Cascades,” Trans. Journal of Basic Engineering, ASME, Vol.82, Sept., pp 575-587.

[4] Dixon, S., 1998, Fluid Mechanics and Thermodynamics of Turbomachinery, Butterworth-Heinemann, Boston.

[5] Wilson. D. G., and T. Korakianitis, 1998, “The Design of High-Efficiency Turbomachinery and Gas Turbines”, Prentice Hall, Inc., Upper Saddle River, NJ, Second Edition.

[6] Johnsen, I. A. and Bullock, R. O., editors, 1965, Aerodynamic Design of Axial Flow Compressors, NASA SP-36, NASA, Washington, DC.

[7] Herrig, L. J., Emery, J. C., and Erwin, J. R., 1957, “Systematic Two-Dimensional Cascade Tests of NACA 65-Series Compressor Blades at Low Speeds,” NACA TN 3916, NACA, Washington, DC.

[8] De Wet, C. L. (2010). Performance of an Axial Flow Helium Compressor under High Through-Flow Conditions (Doctoral Dissertation, Stellenbosch: University of Stellenbosch).

[9] Petersen, H. (1970). The Properties of Helium: Density, Specific Heats, Viscosity, and Thermal Conductivity at Pressures from 1 to 100 bar and from Room Temperature to about 1800 K.

[10] Stroud, L., Miller, J. E., & Brandt, L. W. (1960). Compressibility of Helium at-10° to 130° F. and Pressures to 4000 PSIA. Journal of Chemical and Engineering Data, 5(1), 51-52.

[11] Howell, A. R., 1947, “Fluid Dynamics of Axial Compressors,” (Lectures on the Development of the British Gas Turbine Jet Unit), War Emergency Proc. No. 12, Institution of Mechanical Engineers, London, United Kingdom [American Edition published by the American Society of Mechanical Engineers], pp.441-452.

[12] Walsh, P. P., & Fletcher, P. (2004). Gas Turbine Performance. John Wiley & Sons, (2004): 658.

[13] Lieblein, S., 1959, Loss and Stall Analysis in Compressor Cascades, Journal of Basic Engineering, Vol. 81 (September 1959), pp. 387-400.

[14] Rodriguez, Sal B., et al. Development of Design and Simulation Model and Safety Study of Large-Scale Hydrogen Production Using Nuclear Power, AIChE Conference in Cincinnati. 2005.

[15] Koch, C. C., and L. H. Smith, Jr., 1976, Loss Sources and Magnitudes in Axial-Flow Compressors, Journal of Engineering for Power, Vol. A98, pp. 411-424.

[16] McDonald, C. F. (2012). Helium turbomachinery operating experience from gas turbine power plants and test facilities. Applied Thermal Engineering, 44, 108-142.

[17] Guven, U., & Velidi, G. (2011). Design of a Nuclear Power Plant with Gas Turbine Modular Helium Cooled Reactor. Journal of Nuclear Engineering and Technology, 1, 1-15.

[18] Mattingly, J. D. (Ed.). (1989). Elements of propulsion. Department of Aeronautics, US Air Force Academy.

Biographical Information

Purushotham Balaji earned his Bachelor of Engineering degree in Aeronautical Engineering from Anna University, India in 2013. He has worked on many small-scale projects like radio-controlled aircafts and ground testing of Hybrid propulsion rocket systems. His aptitude for aerodynamics and propulsion led him to pursue his Master of Science in Aerospace Engineering, specializing in propulsion and subsequent induction to the Aerodynamics Research Center (ARC) at The University of Texas at Arlington.

He has worked on performance prediction of Helium Compressors for his master's research and will be extending his research work for Turbines and CFD analysis of turbomachines after graduation.